

The Advanced Virgo Photon Calibrators

D. Estevez^{1,2}, P. Lagabbe², A. Masserot², L. Rolland², M. Seglar-Arroyo², D. Verkindt²

¹ Institut Pluridisciplinaire Hubert CURIEN, 23 rue du loess - BP28 67037 Strasbourg cedex 2, France

² Laboratoire d'Annecy de Physique des Particules (LAPP), Univ. Grenoble Alpes, Universit Savoie Mont Blanc, CNRS/IN2P3, F-74941 Annecy, France

E-mail: dimitri.estevez@iphc.cnrs.fr

Abstract. As the sensitivities of LIGO, Virgo and KAGRA detectors improve, calibration of the interferometers output is becoming more and more important and may impact scientific results. For the observing run O3, Virgo used for the first time photon calibrators (PCal) to calibrate the interferometer, using radiation pressure of a modulated auxiliary laser beam impinging on the Advanced Virgo end mirrors. Those optical devices, also used in LIGO, are now the calibration reference for the global gravitational wave detectors network. The intercalibration of LIGO and Virgo PCals, based on the same *absolute* reference called the Gold Standard, has allowed to remove a systematic bias of 3.92% that would have been present in Virgo calibration using the PCal. The uncertainty budget on the PCal-induced displacement of the end mirrors (NE and WE) of Advanced Virgo has been estimated to be 1.35% for O3a and 1.39% on NE PCal (resp. 1.73% on WE PCal) for O3b. This uncertainty is the limiting one for the global calibration of Advanced Virgo. It is expected to be reduced below $\sim 1\%$ for the next observing runs.

1. Introduction

A gravitational wave interferometric detector like Advanced Virgo needs a stable working point, close to a dark fringe, to detect light variations induced by a gravitational wave [1]. To keep the interferometer on this working point, longitudinal control loops are used, that involve actuators on the mirrors of the interferometer. The reconstruction of the gravitational wave strain $h(t)$ from the dark fringe light power variations requires a precise and accurate measurement of those actuators response which is the aim of the calibration [2].

The Advanced Virgo detector participated in August 2017 to the observation run O2 and allowed the first triple coincident detection of a binary black holes merger [3] and the first detection of a binary neutron stars merger with electromagnetic counterpart [4][5]. During this period, the calibration was using the input laser wavelength as a reference to measure the mirrors electromagnetic actuators response used in the reconstruction of the gravitational wave signal [2][6]. For the O3 observation run, from April 1st 2019 to March 27th 2020, the improved sensitivities of the Advanced LIGO and Advanced Virgo detectors required to reduce the calibration uncertainties on $h(t)$. This motivated the use in Virgo of Photon Calibrators (PCal) as reference to measure the mirrors actuators response [7]. Moreover, PCals are also used on the Advanced LIGO and KAGRA detectors, hence an intercalibration of the global gravitational wave detectors network based on the same reference could be performed [8][7].

After an introduction describing the principle of the PCal, this paper gives in section 2 a detailed description of the PCals that have been implemented on the Advanced Virgo interferometer and describes in section 3 the first work done on PCal intercalibration between Virgo and LIGO. Then, section 4 presents the uncertainty budget on the end mirror displacement induced by an Advanced Virgo PCal, estimated over the full observing run O3. Eventually, the conclusion in section 5 contains also a discussion about the challenge of gravitational wave detectors calibration for the next observing runs.

1.1. Photon Calibrator Principle

The aim of the PCal is to use the radiation pressure of a modulated laser beam, whose output power is well known and controlled, to induce on an end mirror of the interferometer a displacement which translates into a modification of the dark fringe signal at the output port of the interferometer and a measured modification of the reconstructed equivalent gravitational wave strain signal $h(t)$.

The force induced by radiation pressure on the end mirror with a PCal is expressed as:

$$F_{pcal}(f) = \frac{2 \cos(\theta)}{c} P_{end}(f) \quad (1)$$

with θ the angle of incidence of the PCal laser beam impinging on the end mirror, c the speed of light and $P_{end}(f)$ the laser power reflected by the end mirror at the modulated

frequency f . This force generates a displacement of the end mirror which is governed by the mechanical response of the suspended optic. This mechanical response is well approximated (within $\pm 0.1\%$) in the range 10 Hz to 400 Hz by a simple pendulum transfer function with a resonant frequency at 0.6 Hz. This means that the end mirror can be considered as a free mass above 10 Hz with a damping of the oscillation proportional to $[m(2\pi f)^2]^{-1}$, with m the mass of the optic. The induced displacement is thus:

$$x_{pcal}^{free}(f) = -\frac{1}{m(2\pi f)^2} \frac{2 \cos(\theta)}{c} P_{end}(f) \quad (2)$$

As the PCal system is acting on an end mirror of the interferometer, the laser power noise introduces some unwanted displacement at any frequency, thus an additional noise in the sensitivity of the interferometer. Therefore, a digital system to mitigate the laser power noise of the PCal and to stabilize the modulated output power has been implemented, as described in section 2.2, so that the remaining broadband noise does not significantly contribute to the Advanced Virgo sensitivity.

1.2. Mechanical response of the PCal

In practice, Eq. 2 works well for the Advanced Virgo PCal between 10 Hz and 400 Hz. Indeed, contrary to the Advanced LIGO PCal two beams configuration [9], the Advanced Virgo PCal uses a single laser beam impinging the center of the end mirror of the interferometer. Resonant axisymmetric elastic modes of the optic are thus excited and their contribution affects the mechanical transfer function of the PCal above 400 Hz as it has already been demonstrated in [10]. In Advanced Virgo, the *drumhead* mode of the end mirror measured around 7813 Hz is expected to have a significant contribution to the mechanical response of the PCal in the frequency range 400 Hz to 2 kHz. The coupling of the *drumhead* mode with the displacement of the end mirror can be modeled as a second order low-pass filter given by:

$$H_d(f) = \frac{G_d}{1 + \frac{j}{Q_d} \frac{f}{f_d} - \left(\frac{f}{f_d}\right)^2} \quad (3)$$

with G_d the gain of the *drumhead* mode coupling, f_d the resonant frequency of the mode and Q_d the quality factor. The effective displacement of the end mirror sensed by the interferometer is thus driven by the following equation:

$$x_{pcal}(f) = \left[-\frac{1}{m(2\pi f)^2} + H_d(f) \right] \frac{2 \cos(\theta)}{c} P_{end}(f) \quad (4)$$

For convenience we also define the PCal induced strain as:

$$h_{pcal}(f) = \frac{x_{pcal}(f)}{L_0} \quad (5)$$

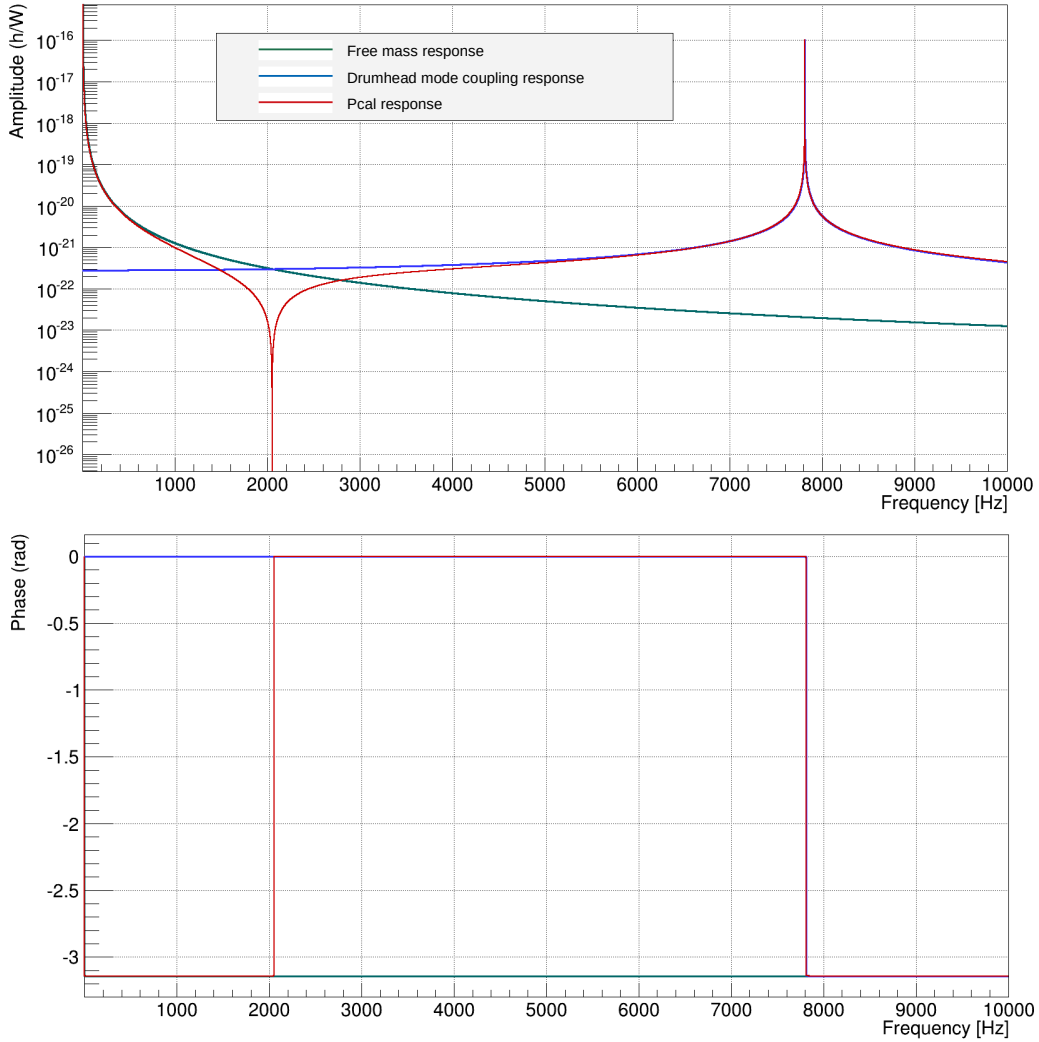


Figure 1: Expected amplitude of the mechanical response of the Advanced Virgo Pcal in strain per watt unit. This PCal response is the complex sum of the free mass response and of the contribution of the *drumhead* mode excitation of the end mirror at 7813 Hz.

where $L_0 = 3000$ m is the nominal length of one arm of the Advanced Virgo interferometer. Figure 1 shows the expected transfer function from the reflected PCal laser power P to the induced end mirror strain h_{pcal} . As the contributions of the free mass response and of the drumhead mode coupling response are in phase opposition between 10 Hz and 7813 Hz, a notch is present at 2050 Hz in the PCal response where the amplitude of the two contributions are equal. This means that the interferometer will not be able to sense any displacement of the end mirror induced by the PCal at this frequency. For frequencies above the notch, the PCal response is enhanced by the *drumhead* mode coupling instead of falling as $\propto f^{-2}$ as it is the case for a free mass.

2. Experimental setup

Two photon calibrators have been installed at the West End (WE) and the North End (NE) stations of the Advanced Virgo interferometer. In addition to being used as reference for the detector's calibration, they allow the verification of the reconstruction of the gravitational wave signal as discussed in section 5.

As shown in Figure 2, each PCal setup is composed of two optical benches. The *injection bench* is used to send the laser beam, stabilized in power by a fast digital control loop, to the inner cavity surface of the end mirror. The *reflection bench* is used to measure the power reflected by the end mirror with a Si photodetector sensitive over 1 cm^2 . The laser beam hits the center of the end mirror with an angle of incidence θ of 18.5° .

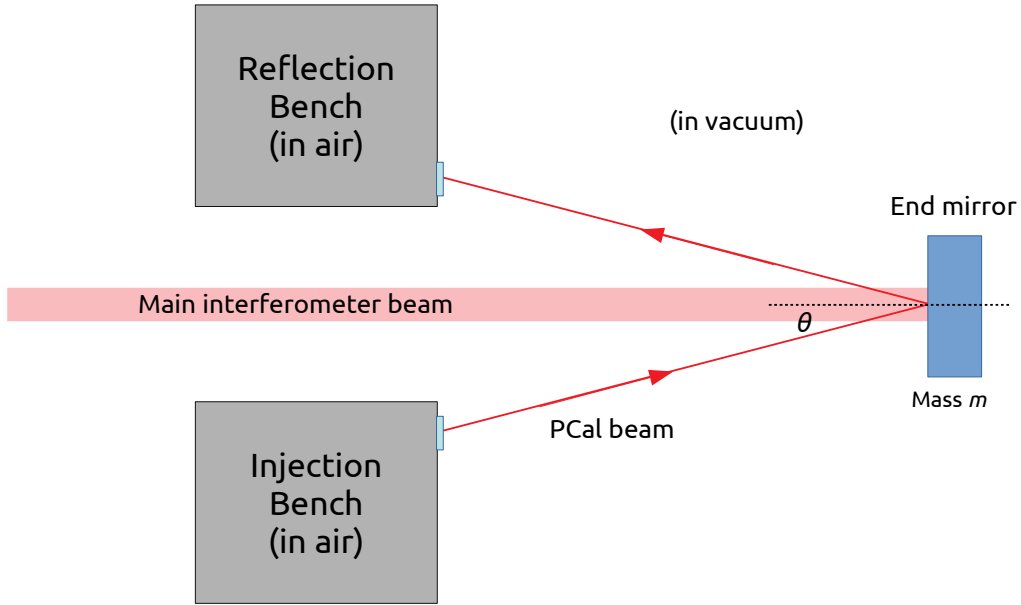


Figure 2: Schematic of an Advanced Virgo photon calibrator viewed from the top.

2.1. Injection and Reflection Benches

As shown in the optical sketch of the injection and reflection benches of Figure 3, the Advanced Virgo PCal laser beam is generated with a diode laser source at 1047 nm . This is the same wavelength as the one used for the Advanced LIGO PCals, which makes easier the laser power intercalibration of both detectors. The PCal laser wavelength is close enough to the main interferometer beam wavelength at 1064 nm which ensures a high reflectivity of the end mirror of the interferometer but it is also different enough so that PCal scattered light does not introduce additional noise in the interferometer.

The range of deliverable power goes from 0 to 3 W hence the PCal operates at 2 W to be able to modulate the power up to ± 1 W and avoid the non linearity near 0. The modulation of the laser power is directly integrated into the laser driver and can be remotely driven through a front panel BNC connector. The beam is brought to the injection bench through an optical fiber and mounted onto a collimator. It is mainly s-polarized but the first optical component on the injection bench is a polarizing beamsplitter cube that transmits the s-polarized beam and reflects the residual p-polarization down to an optical dump. Most of the laser beam (≥ 1.9 W) is then directly sent to the end mirror of the interferometer through a viewport (see section 4.1 for more details) and only a fraction of the beam (~ 5 mW) is monitored by a photodiode named PD1 after a series of mirrors in order to reduce the amount of light reaching the sensor. This photodiode is the *in-loop* sensor used for the Fast Digital Control Loop described in section 2.2 and its calibration is detailed in section 4.1. It is also possible to monitor the optical leverage with a position sensitive detector named PSD1 but it was not used during O3.

The calibration of the photodetectors can be affected by environmental variations of temperature and humidity. Therefore, a thermal sensor and a hygrometer[‡] have been implemented on the injection bench close to PD1 for monitoring.

The reflection bench houses detectors similar to the ones of the injection bench. The PCal laser beam reflected by the end mirror of the interferometer reaches the reflection bench through a viewport similar to the one of the injection bench. Only a small fraction of this beam (~ 5 mW) reaches the photodiode PD2 (and another position sensitive detector called PSD2 which has not been used during O3), whose calibration is described in section 4.1. Prior to PD2, a lens focuses the laser beam that diverged all along the PCal optical layout. For the same reasons as for the injection bench, a thermal sensor and an hygrometer have been mounted close to PD2.

Eventually, the timing of the PCal system can be measured using a remotely controlled LED flashing a GPS synchronized *1 Pulse Per Second* (1PPS) signal onto PD2. Indeed, the photodiode signal is digitally processed and sampled at 20 kHz which induces a delay in the readout. Measuring the delay of the 1PPS signal in the 20 kHz channel allows to calibrate the timing of the PCal, thus the timing of the PCal-induced end mirror motion of the interferometer.

2.2. Fast Digital Control Loop

The Advanced Virgo PCal operates with an input power of 2 W. In this state, inherent fluctuations of power in the laser beam occur at every frequency, inducing a broadband displacement of the end mirror. This laser power noise, converted into strain noise, limits

[‡] The thermal sensor has been implemented at the beginning of O3a (from April 1st 2019 to September 30th 2019) and the hygrometer at the beginning of O3b (from November 1st 2019 to March 27th 2020.)

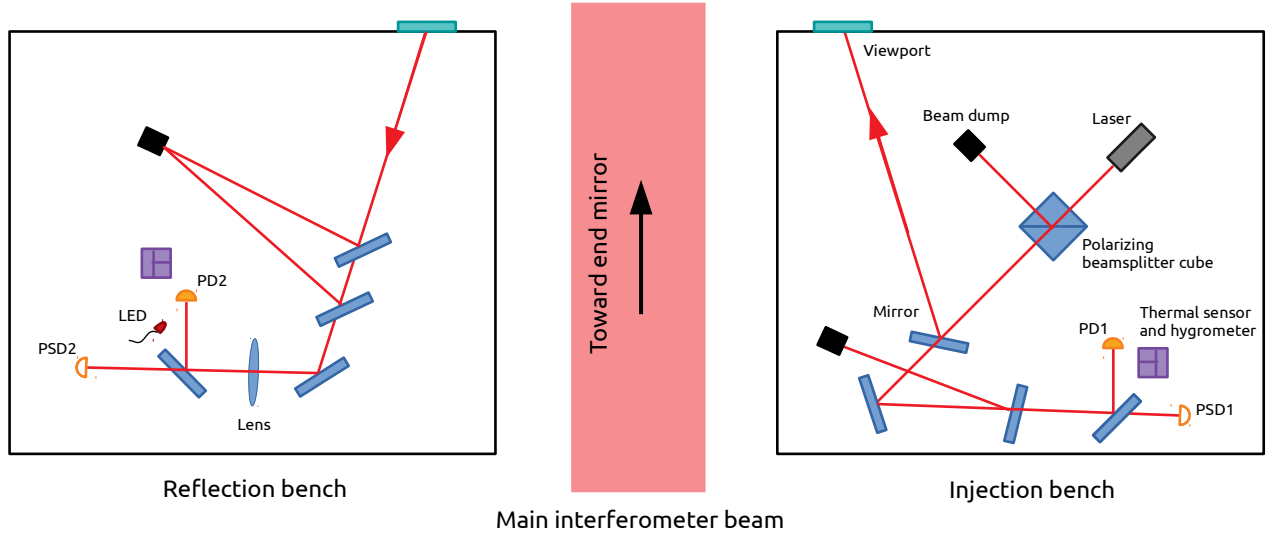


Figure 3: Detailed schematic of an Advanced Virgo photon calibrator viewed from the top. The size of the benches is $40 \text{ cm} \times 40 \text{ cm}$.

the sensitivity of the Advanced Virgo interferometer. Therefore, it has been mitigated to limit its contribution below 10% of the O3 sensitivity.

A fast digital control loop has been implemented to satisfy the above requirement by stabilizing the laser output power at 2 W. This loop is handled by a real-time process running at 200 kHz and using an in-loop output power signal witnessed by the photodiode located on the injection bench. The open-loop and closed-loop transfer functions that characterize the fast control loop have been measured (see Figure 4). The unity gain frequency is close to 4.8 kHz with a phase margin of 57° which ensures a robust control of the system. At 1 kHz the discrepancy between the requested signal and the output signal is -0.2 dB (-5%) and the associated delay is $\tau = 81 \mu\text{s}$ ($phase = -29^\circ$).

The control loop has been running permanently during O3 to stabilize the output power of the laser and to mitigate the laser power noise. Figure 5 shows the PCal laser power noise with and without the control loop. Thanks to the loop, the laser power noise during the O3 run was more than one order of magnitude below the requirement. It is also worth mentioning that there are three spectral lines remaining above the requirements. One of them is the 50 Hz signal coming from the distribution of the mains. The two other lines are permanent sinewave excitations at 36.5 Hz and 60.5 Hz sent to an end mirror of the interferometer by modulating in amplitude the laser power of the PCal. They are used to monitor the calibration of the interferometer and the good reconstruction of the gravitational wave signal. Hence, they need to be clearly visible in the Advanced Virgo sensitivity.

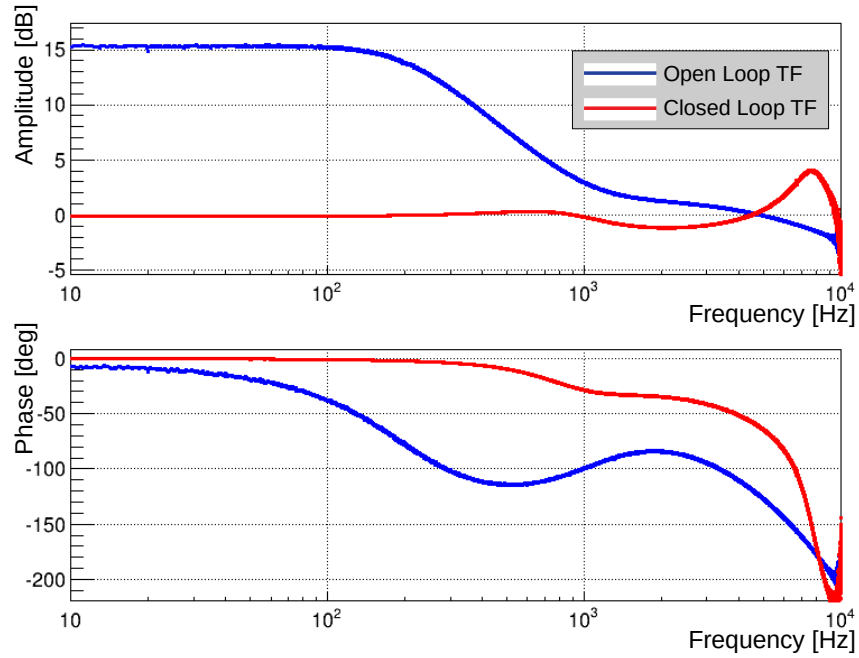


Figure 4: Open-loop (blue) and closed-loop (red) transfer functions of the PCal Fast Digital Control Loop. The measured unity gain frequency is around 4.8 kHz and the phase margin is 57°.

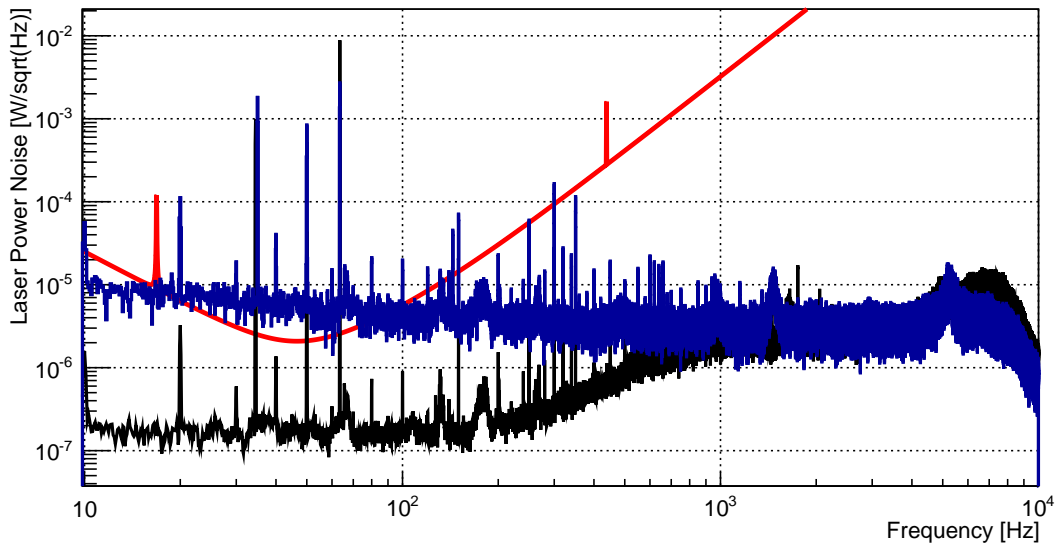


Figure 5: Laser power noise of the Advanced Virgo PCal without control loop (blue) and with control loop (black). The requirement for the laser power noise of the PCal contribution at 10% of the sensitivity for the observing run O3 is shown in red.

2.3. PCal photodiodes

The estimation of the laser power reflected by the end mirror is done using the photodiodes on the injection and reflection benches. To do so, those photodetectors have to be carefully calibrated so that the voltage delivered by the sensor receiving the beam can be translated into effective laser power unit reflected by the end mirror. The method for this calibration procedure is to compare laser power measurements with an integrating sphere, so-called Virgo Integrating Sphere (VIS), on the injection and reflection benches recording the laser beam going into the vacuum tower and the laser beam going out of it. In the same time, the photodiode on the injection bench (PD1) collects a fraction of the light of the laser beam and delivers a certain voltage which is recorded and which can then be converted into power unit using the averaged results of VIS measurements from both benches. Once PD1 has been calibrated, VIS is no longer used to calibrate PD2, and the calibration of PD2 is performed comparing the calibrated laser power measured by PD1 against the voltage delivered by PD2.

Before performing the photodiodes calibration, one needs to be sure that VIS power calibration is *absolute*. In section 3, the *absolute* calibration of VIS is described and this sphere has been used during O3 as the calibration reference for the PCal sensors.

3. Intercalibration with LIGO

One of the main challenge to estimate the displacement of an end mirror of Advanced Virgo induced by a PCal is to determine the PCal laser power reflected by the end mirror. The accuracy on this laser power is the limiting factor of the calibration of the interferometer and impacts the precision of the reconstructed gravitational wave strain provided to data analysis. A pick-off of the reflected laser beam is sensed by photodiode PD2 on the reflection bench and has to be calibrated in an *absolute* manner so that the voltage delivered by the sensor can be precisely converted into absolute power reflected by the end mirror. The calibration of the photodiode is done using the Virgo Integrating Sphere (VIS) which is a Newport 3.3 in. diameter integrating sphere mounted with a 3 mm diameter InGaAs photodetector. The linearity of this detector has been measured to $\pm 0.4\%$ in the range 0.2 W to 3 W. The method to derive the conversion factor of the photodiode from voltage to power is to simultaneously record the PCal laser power with the integrating sphere and the output voltage of PD1, as described in section 2.3. PD2 is then calibrated against PD1 after having removed the integrating sphere of the bench and using the laser beam hitting simultaneously both photodiodes. This procedure requires an *absolute* calibration of the Virgo integrating sphere by carefully choosing an *absolute* calibration reference which is the LIGO Gold Standard (GS) calibrated by the National Institute of Standards and Technology (NIST) in Boulder, CO. [11].

Since LIGO and Virgo are performing a coincident analysis of the calibrated gravitational

wave data stream provided by each interferometer, one has to be sure that the relative calibration between each detector does not introduce any bias in the analysis or that at least the putative bias is as small as possible. During the observing run O2, the Free Swinging Michelson technique was used as a reference for Virgo calibration and could not be directly compared to LIGO calibration based on the PCal [12]. Indeed, the *absolute* reference for LIGO was the Gold Standard and the one for Virgo was the wavelength of the main interferometer laser beam. The decision to use the PCal on Virgo for the observing run O3 was then motivated by the different upgrades performed on the setup which allowed to be confident on its calibration, stability and precision. The use of the PCal was also motivated by the possibility to intercalibrate the PCal laser power between LIGO and Virgo with the Gold Standard. Figure 6 shows the calibration chain from GS to the PCal power sensors located on the injection and reflection benches of the Advanced Virgo interferometer and also the optical setup to calibrate VIS against GS.

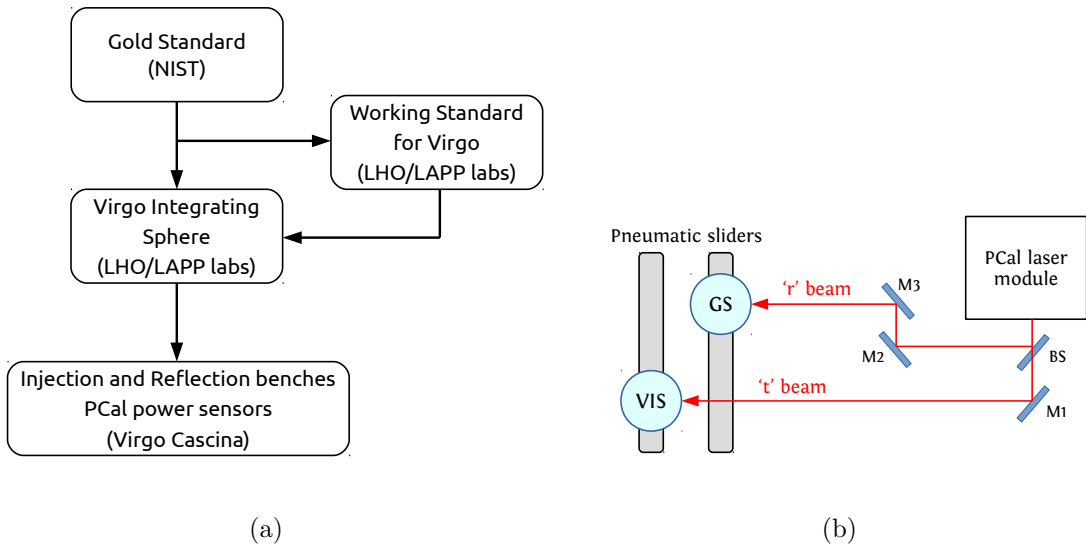


Figure 6: (a) Diagram of the calibration chain made for the laser power calibration of the Advanced Virgo PCal. The LIGO Gold Standard calibrated by NIST stands at the top of the chain and serves as *absolute* reference for the Advanced Virgo PCal power sensors at the bottom of the chain. The location given in brackets indicate where the calibration measurements were performed. (b) Schematic of the optical setup used to calibrate the Virgo Integrating Sphere against the Gold Standard. A PCal laser module is used to generate a laser beam which is then split into two beams with a beamsplitter (BS). The Gold Standard and the Virgo Integrating Sphere are mounted on pneumatic sliders to swap between the reflected (r) and transmitted (t) beams to determine the ratio of the responsivities. This setup is also used to calibrate the Working Standards of Advanced LIGO and KAGRA.

3.1. Calibration of the Virgo Integrating Sphere

The calibration of VIS against GS consists in measuring:

$$\Gamma_{VIS/GS} = \frac{\rho_{VIS}}{\rho_{GS}} \quad (6)$$

which is the ratio of the integrating spheres responsivities ρ . The calibration factor $\Gamma_{VIS/GS}$ has been computed as follows:

$$\Gamma_{VIS/GS} = \sqrt{\frac{(P_{VIS,r} - P_{VIS,r}^{BG}) \cdot (P_{VIS,t} - P_{VIS,t}^{BG})}{(P_{GS,r} - P_{GS,r}^{BG}) \cdot (P_{GS,t} - P_{GS,t}^{BG})}} \quad (7)$$

with r and t standing for the reflected and transmitted beam respectively which denotes the position of the spheres on the pneumatic sliders from Figure 6(b). P stands for the measured powers with incoming laser beam and BG indicates the background measurements with the laser turned off that are subtracted to the measured laser power values. Doing ratios of power measured by GS and VIS eliminates simultaneous laser power variations and swapping their position eliminates the effect of beamsplitter imperfections. As a result this procedure gives access to the ratio of the integrating spheres responsivities ρ .

The calibration factor has been computed for five series of measurements performed at LHO in February 2019 on five different days and the results are shown in Figure 7. The average of those measurements is $\bar{\Gamma}_{VIS/GS} = 0.9623 \pm 0.1\%$ taking into account the dispersion of the points as a systematic uncertainty. The uncertainty on the linearity of the readout of VIS ($\pm 0.4\%$) and the uncertainty on the *absolute* calibration factor measured by NIST for GS ($\pm 0.32\%$) are then added quadratically to the previous uncertainty to give a final estimation of the responsivities ratio $\bar{\Gamma}_{VIS/GS} = 0.9623 \pm 0.52\%$. This indicates that the power measured by VIS was off by almost 4% compared to the power read by GS. For the O3 run, the laser power of the Advanced Virgo photon calibrators were thus calibrated with VIS corrected by $\bar{\Gamma}_{VIS/GS}$.

3.2. Calibration of the Working Standard for Virgo

Since VIS is used on Virgo to calibrate the PCal it cannot be compared against GS (which stays at LHO) as often as needed to check the stability of the calibration factor. A Working Standard for Virgo (WSV) similar to the Working Standards used on LIGO and KAGRA has thus been mounted at LHO with the aim of staying at LAPP§, where the Virgo PCal is developed, so that VIS could be compared against WSV during O3. This integrating sphere WSV was calibrated against GS with the same setup used to calibrate VIS. Figure 8 shows the calibration factor corresponding to the ratio of the responsivities of WSV and GS computed as in equation 7 for six series of measurements performed at LHO in February

§ Laboratoire d'Annecy de Physique des Particules

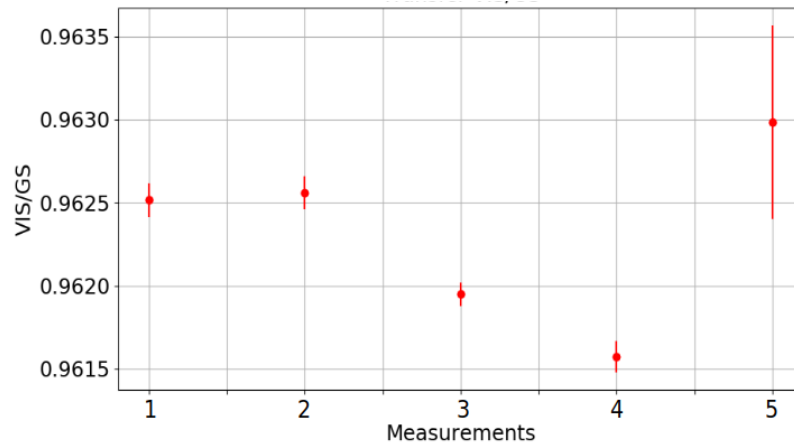


Figure 7: Calibration factors between the Gold Standard and the Virgo Integrating Sphere. The five points have been measured by averaging 30 sets of 100 s measurements at a fixed laser power $P \sim 0.4$ W on five different days at LHO in February 2019. Only statistical errors are shown. The fifth point has larger error bars suspected to be the consequence of unexpected fluctuations of the laser power servo control.

2019 on six different days. The averaged calibration factor is $\bar{\Gamma}_{WSV/GS} = 0.5613 \pm 0.34\%$ with systematic uncertainties. For technical reasons, the ratio is not close to 1 since the photodiode transimpedance of WSV has been divided by a factor 2 compared to the one of GS in order to meet the requirements of Advanced Virgo PCal laser power.

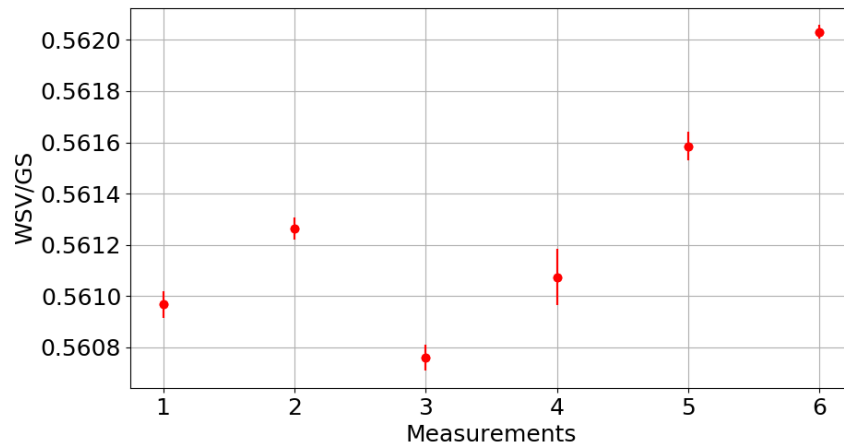


Figure 8: Calibration factors between the Gold Standard and the Working Standard for Virgo. The six points have been measured by averaging 30 sets of 100 s measurements at $P \sim 0.4$ W on six different days at LHO in February 2019. Only statistical errors are shown.

3.3. Intercalibration stability

The ratio of the responsivities of VIS and WSV has also been measured at LHO in the same experimental conditions as for the previous ratios described in the above sections. The value of this ratio is the reference from which the stability of VIS calibration is estimated and has to be monitored at LAPP during O3. Therefore, a similar optical setup to calibrate the integrating spheres as the one at LHO has been mounted at LAPP during O3 to check the stability of VIS calibration. Since the acquisition tools are different from LHO to LAPP we used a voltage calibrator to calibrate our voltage readout at LAPP at the level of 0.007%. Figure 9 shows the four measurements of $\Gamma_{VIS/WSV}$ performed at LHO in February 2019 and the five measurements performed at LAPP in June and October 2019. The dispersion of the points around the mean value is $\pm 0.5\%$ which is thus the value used during O3 to characterize the stability in time of the intercalibration between LIGO and Virgo.

Investigations to understand the systematic uncertainties related to these measurements are needed for the next observation run O4 in order to find solutions to improve the stability in time of the intercalibration. More measurements of Virgo spheres against the Gold Standard will also have to be performed to strengthen the confidence in the calibration factors.

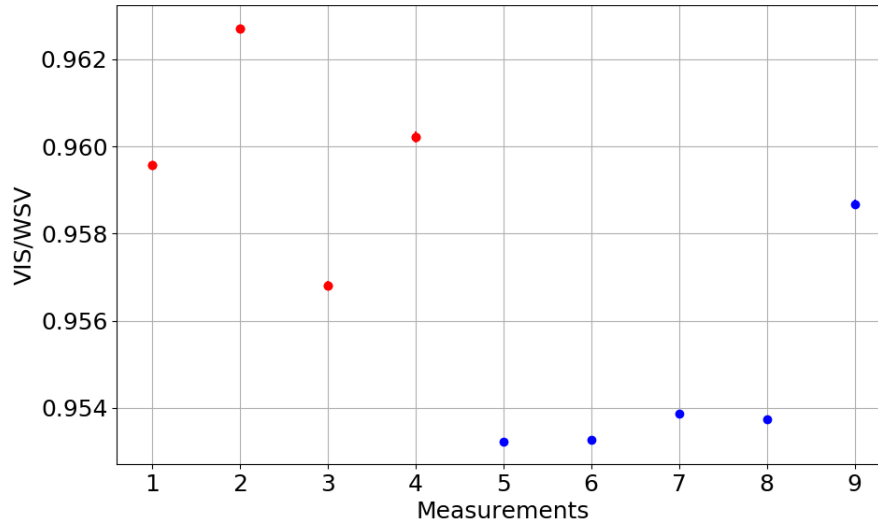


Figure 9: Calibration factors between the Working Standard for Virgo and the Virgo Integrating Sphere. The red points have been measured by averaging 30 sets of 100 s measurements at $P \sim 0.4$ W on four different days at LHO in February 2019. The blue points have been measured by averaging 1 set of 3600 s measurements at a fixed laser power $P \sim 1$ W on five different days at LAPP (four days in June 2019 and one day in October 2019). Only statistical errors are shown.

4. Uncertainties

The total uncertainty on the end mirror displacement induced by the PCal arises from the determination of all the parameters from equation 4. The main contribution to this total uncertainty comes from the estimation of the laser power reflected by the end mirror. Indeed, many factors have to be taken into account from the *absolute* calibration of VIS with GS down to the Advanced Virgo PCal sensors calibration.

4.1. Calibration of the PCal photodiodes

The power measurements on the injection and reflection benches with VIS to calibrate the photodiodes are done outside the vacuum tower containing the end mirror. The laser beam is thus affected by the optical losses of the viewports between the tower and the PCal benches. Hence, to precisely estimate the power reflected by the ETM, the viewport losses have to be characterized.

The viewports are coated on both in-air and in-vacuum surfaces with 1064 nm broadband anti-reflective coatings whose power reflectivity had been estimated to be around $R = 0.05\%$ per coating at 1047 nm. The absorption of the viewports is negligible compared to their reflectivity so that one can reasonably assume that all the losses come from the reflected light. Moreover, the power reflectivity coefficient of the end mirror at 1047 nm is higher than 99.99% and is thus not affecting the total optical efficiency of the PCal. Therefore, the power reflected by the end mirror P_{end} can be expressed as:

$$P_{end} = P_{inj}(1 - R)^2 = \frac{P_{ref}}{(1 - R)^2} \quad (8)$$

where P_{inj} and P_{ref} are the laser power respectively measured on the injection and reflection benches. P_{end} can thus be approximated, at the first order, as the average of P_{inj} and P_{ref} . This is what has been used for the photodiodes calibration. We expect the optical efficiency $\eta = P_{ref}/P_{inj}$ to be around 0.998 considering the viewport losses meaning that the uncertainty on P_{end} should be within 0.2%.

However, when the measurements were performed it was found that the measured laser power on the injection bench was varying at maximum by 0.8%, depending on the position of VIS between the viewport and the last mirror before the viewport. On the reflection bench, the measured laser power did not depend on the position of VIS between the viewport and the first mirror of the reflection bench. The main difference between these two measurements is the size of the laser beam which is bigger at the reflection bench. We thus expect that if the beam size is smaller than a specific size, a non negligible amount of light entering VIS is reflected back outside the sphere. This effect would give an under estimation of the measured power. We found indeed a position on the injection bench where the power was almost 0.5% smaller than the power on the reflection bench and another position where the power was

0.3% higher. The measurements were thus performed with VIS located where the beam size is the largest on the injection bench, and the laser power was then 0.3% higher than the power measured on the reflection bench which is closer to the value we would expect from the optical efficiency.

Since we could not estimate properly the optical efficiency of the PCal due to the effect mentioned above, we decided to keep a conservative uncertainty of 1% for this measurement resulting from 0.8% due to power variations depending on VIS position plus 0.2% considering the expected optical efficiency. This is the dominant uncertainty in the final error budget of the PCal and it will have to be tackled and characterized more accurately in the future. A possible study would be to measure the laser power with VIS at different positions on an optical bench and with different laser beam sizes.

Table 1 summarizes the sources of systematic uncertainties on the estimation of the PCal laser power reflected by the end mirror of the interferometer, from the top (the Gold Standard) to the bottom (the PCal sensors) of the laser power calibration chain. Then, the total relative uncertainty on P_{end} is computed as:

$$\frac{\sigma_P}{P_{end}} = \left[\sum_i \left(\frac{\sigma_{x_i}}{x_i} \right)^2 \right]^{1/2} \quad (9)$$

with x_i the different parameters estimated as sources of systematic uncertainties in the laser power calibration chain.

Parameter	1σ Uncertainty
GS responsivity (2018)	0.32%
VIS linearity	0.4%
VIS/GS responsivity ratio	0.1%
VIS/WSV responsivity ratio	0.5%
Voltage calibrator	0.007%
VIS position and optical efficiency	1%
Power reflected by the end mirror	1.24%

Table 1: Summary of the sources of systematic uncertainty on the estimation of the PCal laser power reflected by the end mirror of the interferometer.

4.2. Geometrical parameters

The geometrical parameters are also contributing to the overall uncertainty on the end mirror displacement. Above the resonant frequency of the end mirror suspension, the displacement of the optics induced by a PCal is inversely proportional to the mass of the optics. In Advanced Virgo, the mass has been measured to 42.30 ± 0.02 kg which gives a 1σ uncertainty

of $\pm 0.05\%$ on the PCal-induced end mirror displacement.

The angle of incidence of the PCal laser beam hitting the end mirror has been evaluated, with optomechanical constraints from the drawings, to be $\theta = 18.5^\circ$. This angle is limited by the diameter of the viewports. This diameter is 63 mm and the beam has been centered on the viewports better than ± 10 mm. The 1σ uncertainty on the angle of incidence is thus treated as a Type-B uncertainty [13] contributing in the cosine as $\pm 0.12\%$.

Unwanted rotation of the end mirror can be caused by a torque induced by a miscentering of the PCal laser beam and the main interferometer laser beam as shown in Figure 10(a). This effect changes Eq. 4 by adding an end mirror rotation term as follows:

$$x_{pcal}(f) = -\frac{1}{m(2\pi f)^2} \frac{2 \cos(\theta)}{c} H(f) P(f) \left(1 + \frac{\vec{a} \cdot \vec{b} m}{I} \right) \quad (10)$$

where I is the rotational moment of inertia of the end mirror of mass m and \vec{a} (resp. \vec{b}) is the vector from the center of the mirror to the position of the main interferometer laser beam spot (resp. PCal laser beam spot) on the optic. In Advanced Virgo, the centering of the main interferometer beam is controlled to be better than ± 0.5 mm and the PCal laser beam is centered better than ± 20 mm due to optomechanical constraints. Considering the worst case scenario where the scalar product between the two vectors is extremum (both beam spots are shifted in the same direction), the miscentering of the beams leads to a relative error of $\pm 0.001\%$ on the displacement of the end mirror due to the tilt of the optics.

Eventually, Table 2 summarizes the uncertainties arising from the geometrical parameters of the PCal-induced end mirror motion equation.

Parameter	1σ uncertainty
Mass of the end mirror	0.05%
Angle of incidence (cosine)	0.12%
Rotation of the optic	0.001%
Total	0.13%

Table 2: Summary of the sources of systematic uncertainties on the geometrical parameters of the PCal-induced end mirror motion equation.

4.3. Mechanical response of the PCal

As mentioned in previous sections, the PCal laser beam hits the center of the end mirror of the interferometer and thus excites axisymmetric internal modes of the optic. The model of the PCal-induced motion of the end mirror is given by Eq. 4 where $H(f)$ is the last item

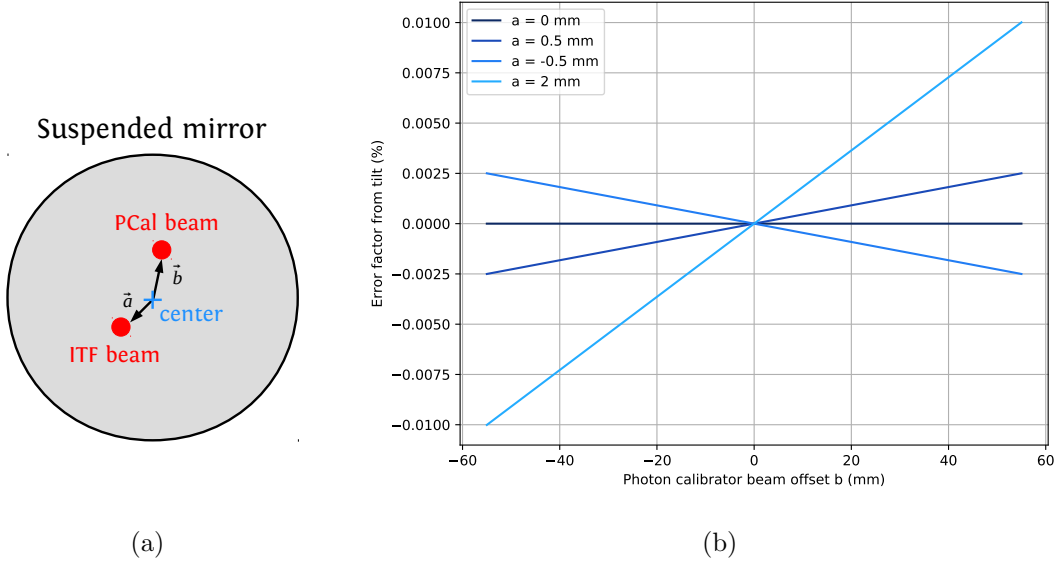


Figure 10: (a) Schematic of a suspended end mirror of the interferometer with the main interferometer (ITF) laser beam and the PCal laser beam spots shifted from the center of the optics by \vec{a} and \vec{b} respectively. The miscentering of the beams is exaggerated in this figure for clarity purpose. (b) Relative error on the end mirror displacement due the tilt of the optics induced by a miscentering of the main interferometer beam and the PCal beam. The vectors positioning the beams are assumed to be collinear in order to maximize the error.

of the equation that we have to characterize. The value of the *drumhead* mode f_d has been measured to be 7812.8 ± 1.1 Hz for the WE mirror and 7813.2 ± 0.5 Hz for the NE mirror. As these frequencies depend on the temperature surrounding the end mirrors their associated uncertainty has been estimated by considering the distribution of temperature of the TCS ring heaters during O3 using a measured dependency of 0.88 Hz/ $^{\circ}$ C and by considering the reference temperature during the measurements of f_d . The maximum deviation of temperature from the reference temperature during the measurements is 1.2° C for WE and 0.6° C for NE. These temperature variations lead to a relative uncertainty on f_d of $\pm 0.014\%$ for WE and $\pm 0.006\%$ for NE. The value of the quality factor Q_d is of the order of 10^6 which is high enough so that an error of a few percent on this value has a negligible contribution on the global uncertainty of $H(f)$.

The last parameter for which an uncertainty has to be estimated is the gain of the *drumhead* mode G_d . The measurement of this gain has been done by measuring the frequency of the notch in the mechanical response of the PCal around 2 kHz as shown in the simulated response in Figure 1. Indeed, the notch is the result of the free-mass response having the same amplitude as the internal deformation of the mirror but in phase opposition. The idea

is thus to compare a PCal-induced strain h_{pcal} on the end mirror, taking into account only the simple pendulum model H_p , with the reconstructed strain of Advanced Virgo interferometer h_{rec} . Taking the transfer function from the PCal strain to the reconstructed strain will reveal the discrepancy between both strains which arise from the unmodeled *drumhead* mode. It is important to notice that this measurement depends on the reconstruction of the gravitational wave strain and may introduce unwanted bias in the measurement. We thus assume that if there is a bias in h_{rec} around the notch frequency band it is a constant bias on the amplitude and it is not frequency dependent so that the shape of the measurements is unchanged. The quantity that we want to measure and fit can be expressed as:

$$\frac{h_{rec}}{h_{pcal}} \propto \frac{H_p + H_d}{H_p} \propto G_0 \left(1 - \frac{f^2}{\lambda^2 \left(1 - \left(\frac{f}{f_d} \right)^2 \right)} \right) \quad (11)$$

$$(12)$$

where G_0 and λ are the two parameters of the fit. The parameter λ is linked to the notch frequency f_n by the following relation:

$$f_n = \frac{\lambda f_d}{\sqrt{\lambda^2 + f_d^2}} \quad (13)$$

Since the gain of the *drumhead* mode coupling response at the frequency f_n is not equal to the static gain ($f = 0$) of the coupling, we have introduced λ which is the equivalent frequency where the amplitude of the free-mass response is equal to the static gain of the *drumhead* mode coupling. Fitting for λ instead of f_n gives us directly the static gain G_d in meter per newton expressed as:

$$G_d = \frac{1}{4\pi^2 m \lambda^2} \quad (14)$$

Figure 11 shows the amplitude of the transfer function for both WE and NE PCals. The gain of the *drumhead* mode coupling response for both PCals have been renormalized in unit of strain per watt for convenience and have been estimated to:

$$G_d^{WE} = (2.82 \pm 0.01) \times 10^{-22} \text{ h/W}$$

$$G_d^{NE} = (2.78 \pm 0.01) \times 10^{-22} \text{ h/W}$$

The parameters of the *drumhead* mode coupling for both end PCals are then known and the resulting uncertainties are gathered in Table 3. One can notice that those uncertainties add a frequency dependent contribution to the global uncertainty budget of the PCal-induced end mirror motion.

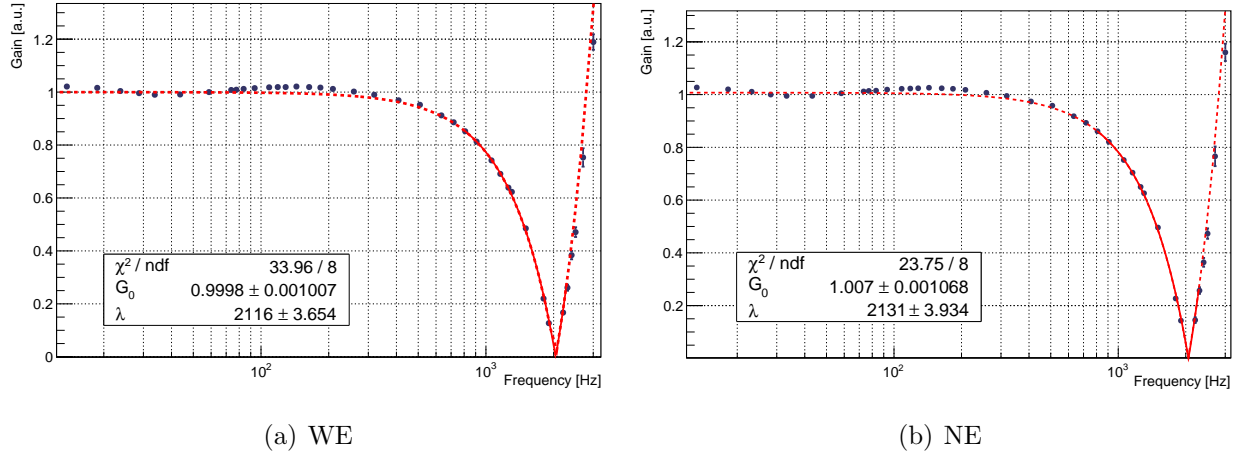


Figure 11: Measured amplitude of h_{rec}/h_{pcal} for WE PCal (a) (NE PCal (b)) and the associated fit.

PCal	ΔG_d	Δf_d
WE	$\pm 0.35\%$	$\pm 0.014\%$
NE	$\pm 0.37\%$	$\pm 0.006\%$

Table 3: Uncertainty on G_d and f_d for WE and NE PCal mechanical responses.

4.4. Stability during O3a and O3b

The calibration of the PCal photodiodes has been monitored during O3 to look for any other sources of systematic uncertainties and to check the calibration stability in time. The responsivity of the Advanced Virgo PCal photodiodes depends on the temperature as $0.5\%/^{\circ}\text{C}$ at 1047 nm. A monitoring of the surrounding temperature during O3 has thus been done to evaluate the impact on the overall PCal uncertainty budget. Since the temperature variations do not follow a gaussian distribution we treated the change in photodiode responsivity as a Type-B uncertainty assuming a rectangular distribution of temperatures over the whole range of variations. The highest range of temperature variations was found to be 0.65°C on NE PCal *reflection bench* which resulted in a Type-B uncertainty of $\pm 0.1\%$ on the photodiode calibration, to be added to the PCal uncertainty budget.

Some variations of photodiodes power calibration larger than the expected ones due to temperature variations were seen between PD1 and PD2 during O3a as shown in Figure 12.

The monitoring and the analysis of these variations were done using *calibration lines* of the PCal. Those lines are sinewave excitations sent to the end mirrors of the interferometer by modulating in amplitude the laser beam of the PCal. A long term study was done over O3a comparing the reconstructed signal h_{rec} from the output of the interferometer against

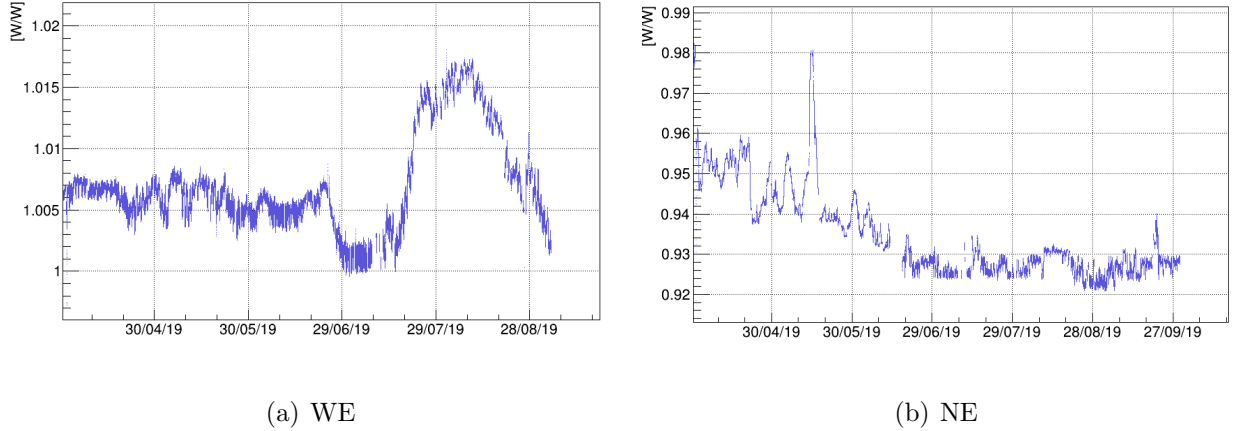


Figure 12: Ratio of PD1 and PD2 signals over O3a at the frequency of the calibration lines. (a) The calibration line frequency is 60.5 Hz on WE and (b) 63.5 Hz on NE.

the signal h_{pcal} reconstructed from the PCal photodiodes. Figure 13 shows the ratio of h_{rec} over h_{pcal} for both photodiodes on both PCals during O3a. The photodiodes PD2 on WE and PD1 on NE are the two photodiodes that contribute the most to the variations seen on Figure 12. Only the photodiodes PD1 on WE and PD2 on NE were thus used to estimate the PCal-induced end mirrors motion during O3. The uncertainty on their calibration stability has been assessed using the width of the distributions of h_{rec} over h_{pcal} . Figure 14 shows these distributions for O3a and O3b. Those distributions account for calibration variations of h_{pcal} but also the ones of h_{rec} , thus only an upper limit on the uncertainty on the h_{pcal} stability can be drawn from this analysis. Therefore the 1σ uncertainty on the stability of the photodiodes power calibration has been conservatively estimated to $\pm 0.5\%$ over the O3a period.

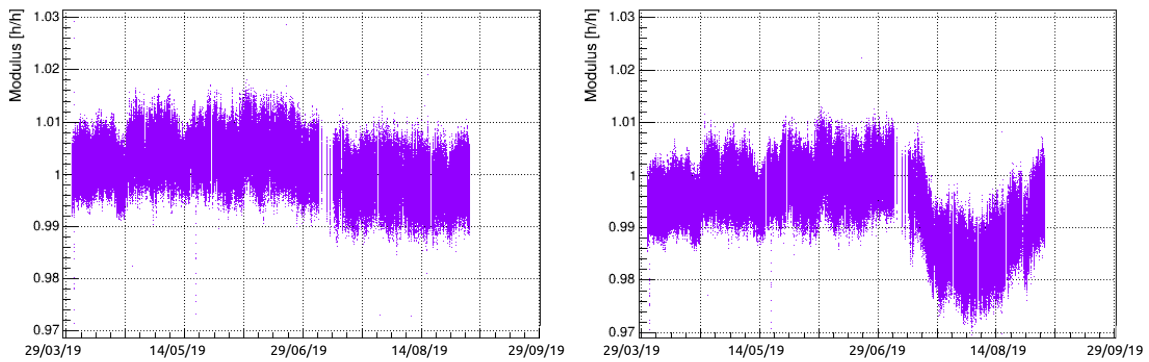
In between O3a and O3b^{||}, the NE and WE driver lasers had to be repaired after an electrical failure. Only the WE driver laser was mounted back in time for the start of O3b and the NE driver laser has been reinstalled later during O3b in January 2020. A few days before O3b, the WE PCal set-up had to be realigned and WE PD1 recalibrated. The new measured calibration factor for WE PD1 differed by +1.3% from the one of O3a. This difference exceeds the uncertainty of 0.8% stated in Section 4.1 due to VIS positioning on the optical bench and therefore was significant enough to be corrected for O3b. One can see in Figures 14(a) and 14(c) that the mean values of the distributions differ by $\sim 1.7\%$ and with similar standard deviations of 0.5%. It has been found that this difference between both distributions is due to the recalibration of WE PD1 and to relative humidity changes. We thus chose to extend the uncertainty on the WE PCal PD1 calibration from 0.5% for O3a to

^{||} One month break in the observation run of LIGO and Virgo from October 1st to November 1st 2019.

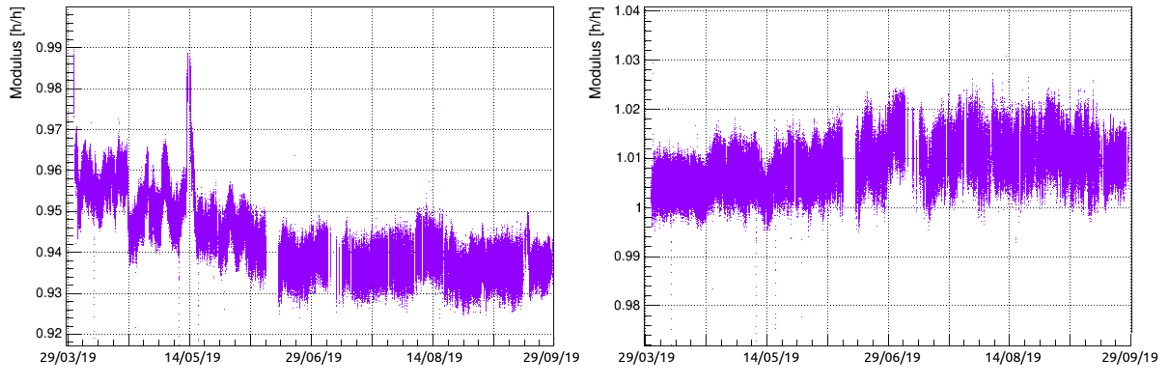
1.2% for O3b as explained further in this section.

NE driver laser was mounted back on the 21st of January 2020 but not recalibrated to be able to compare the new set-up to the previous one and also with WE PCal. Figures 14(b) and 14(d) show that the mean values between both distributions differ by 0.5% with similar standard deviations of 0.5%. Both distributions being compatible without performing any recalibration of the photodiodes we added them together to get the uncertainty on the stability of NE PCal for O3b which becomes 0.6%.

Table 4 summarizes the uncertainty contributions of the temperature variations and *other sources* that affect the PCal laser power stability.



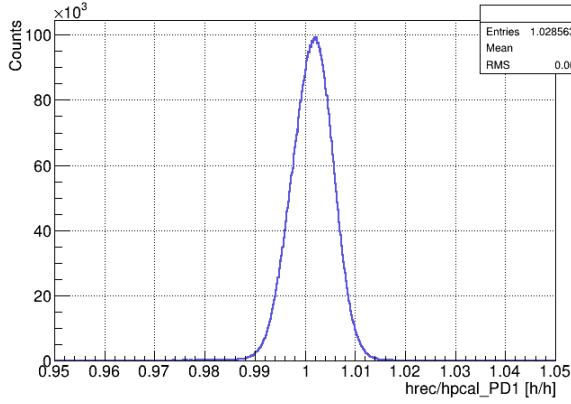
(a) WE PD1 (left) and WE PD2 (right).



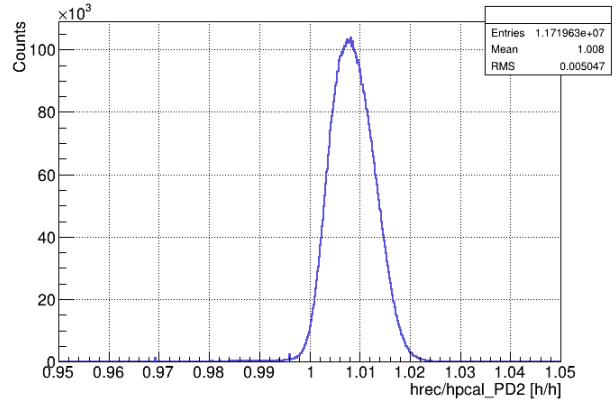
(b) NE PD1 (left) and NE PD2 (right).

Figure 13: Ratio of h_{rec} and h_{pcal} for both PD1 and PD2 signals on both PCals at the frequency of the calibration lines during O3a. (a) Calibration line frequency is 60.5 Hz for WE and (b) 63.5 Hz for NE.

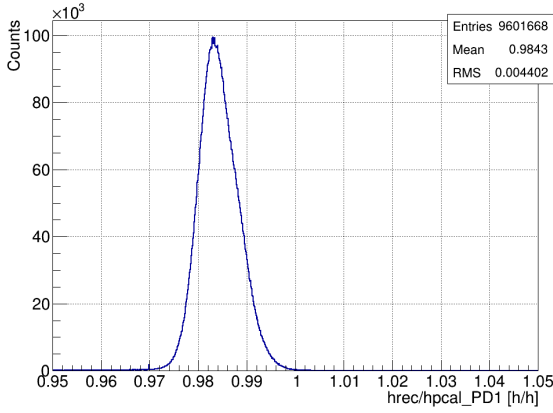
Investigations to understand the *other sources* of variations which affect the stability in time of the PCal calibration have shown that the relative humidity variations around the



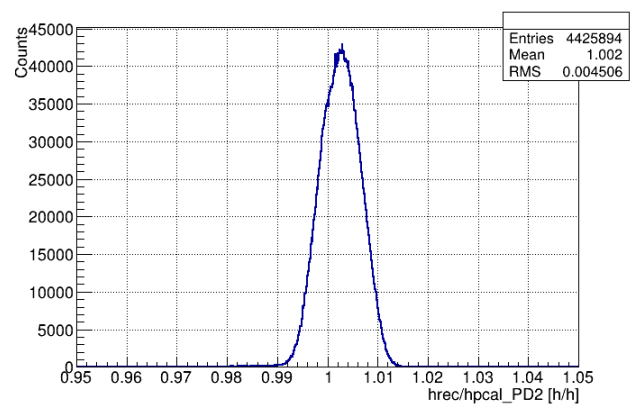
(a) WE PD1 O3a



(b) NE PD2 O3a



(c) WE PD1 O3b



(d) NE PD2 O3b

Figure 14: Distribution of h_{rec}/h_{pcal} using (a) WE PD1 and (b) NE PD2 during O3a and (c) WE PD2 and (d) NE PD2 during O3b. The standard deviation of the distributions is $\sim 0.5\%$ and gives an upper limit on the stability of the PCal calibration over O3a and O3b for a given calibration of the photodiodes.

PCal benches are correlated with the photodiodes calibration variations.

Relative humidity variations affecting the PCal calibration

We have observed that the variations of humidity inside the NE PCal bench was correlated with the NE PD1 signal during O3a and O3b as shown in Figure 15. The correlation varies in time and the behaviors during O3a and O3b are different. During O3a, at least two bands of correlation can be seen whereas during O3b a phenomenon of hysteresis has been

Parameter	1 σ uncertainty O3a		1 σ uncertainty O3b	
	NE	WE	NE	WE
Responsivity (temperature)	$\pm 0.1\%$	$\pm 0.1\%$	$\pm 0.1\%$	$\pm 0.1\%$
Other sources	$\pm 0.5\%$	$\pm 0.5\%$	$\pm 0.6\%$	$\pm 1.2\%$
Total	0.51%	0.51%	$\pm 0.61\%$	$\pm 1.2\%$

Table 4: Uncertainty on the stability in time of the PCal-induced end mirror displacement due to temperature-dependent photodiode response and other sources of uncertainty during O3.

put in evidence. We thus suspect that the change in relative humidity is the main source of the amplitude variations of the NE PCal photodiode response up to $\sim 13\%$. However the variations of NE PD2 signal with respect to humidity variations are consistent with the 0.5% and 0.6% uncertainty estimated for the stability in time of its calibration over O3a and O3b.

Similar investigations have been performed on WE PCal photodiodes and are shown in Figure 16. During O3a, WE PD1 signal variations due to humidity changes are consistent with the 0.5% uncertainty given for its calibration stability in time. It is also noticeable that the main part of the 1.5% variations of WE PD2 signal during O3a is not correlated with humidity changes and that humidity variations may count only for 0.5% of the WE PD2 photodiode calibration variations. Regarding O3b, the variations of WE PD2 signal due to humidity changes were also within $\sim 0.5\%$.

After the recalibration of WE PD1 (+1.3%) performed with a relative humidity of 60% before O3b, the value of h_{rec}/h_{pcal} differed by 0.5% with the one of O3a at the same relative humidity (see Figures 16(a) and 16(c)). This indicates that the calibration measurements of WE PD1 performed before O3a and a few days before O3b are coherent and compatible with the uncertainty of 0.8% on VIS positioning on the optical bench. However, during O3b, WE PD1 calibration started to drift by $\sim 1.1\%$ due to humidity variations. Adding quadratically the uncertainty of 0.5% around the mean value, the uncertainty on WE PCal calibration stability for O3b has been increased to 1.2%.

4.5. Error budget

Below the notch frequency, the total uncertainty on the NE (resp. WE) photon calibrators has been estimated to be 1.35% (resp. 1.35%) for O3a and 1.39% (resp. 1.73%) for O3b. The detailed contributions to this uncertainty have been given in the previous sections and are summarized in Table 5. For frequencies above the notch frequency, the interaction with the mirror drumhead mode must be taken into account and the PCal uncertainty is frequency dependent. Figure 17 shows the global frequency dependent uncertainty budget on WE and NE PCal for O3a.

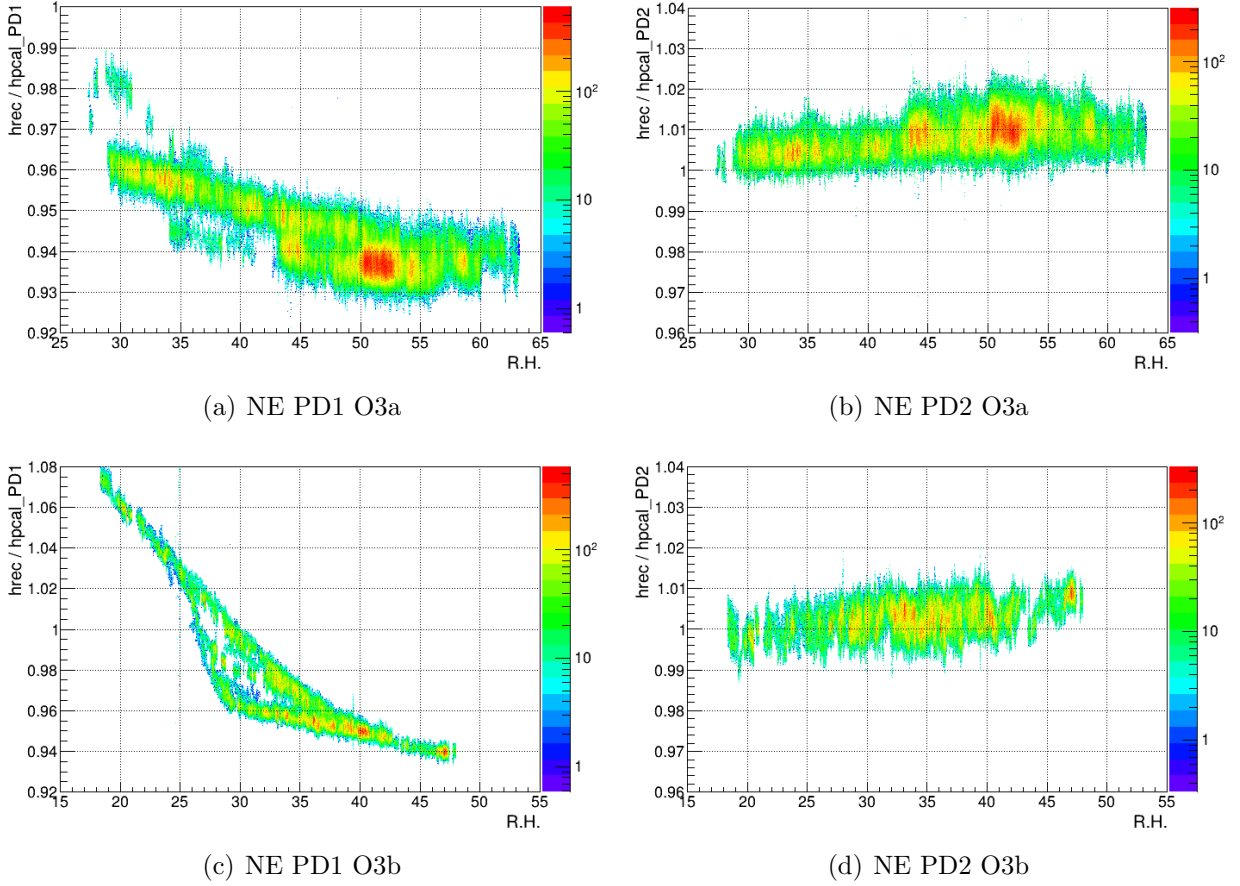


Figure 15: Distribution of h_{rec}/h_{pcal} for NE PCal photodiodes as a function of relative humidity (R.H.) surrounding NE PCal during O3a and O3b.

Parameter	1σ uncertainty O3a		1σ uncertainty O3b	
	NE	WE	NE	WE
Reflected laser power (P)	1.24%	1.24%	1.24%	1.24%
Geometrical parameters	0.13%	0.13%	0.13%	0.13%
Calibration stability (O3)	0.51%	0.51%	0.61%	1.2%
Total	1.35%	1.35%	1.39%	1.73%

Table 5: Uncertainty budget of the photon calibrators below 1500 Hz.

In addition, a PCal timing uncertainty must be taken into account. Indeed, the signal measured by the photodiode to estimate the laser power reflected onto the end mirror is processed by a sensing path and is thus delayed. Thanks to the measurements done with the 1PPS signal sent with a flashing light diode (see section 2.1), this delay has been estimated to

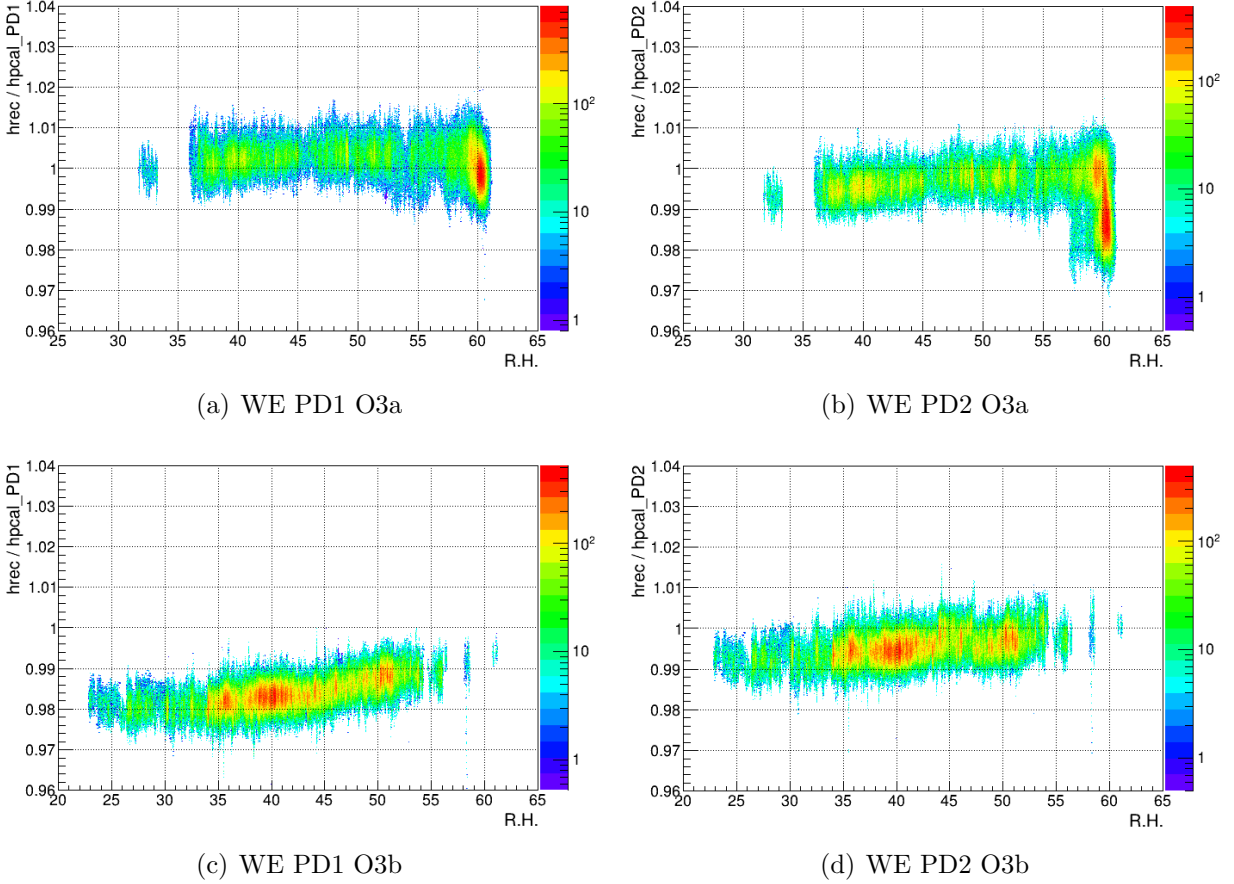


Figure 16: Distribution of h_{rec}/h_{pcal} for WE PCal photodiodes as a function of the relative humidity (R.H.) surrounding WE PCal during O3a and O3b.

be $110 \pm 3 \mu\text{s}$. This delay has been corrected to get the absolute timing of the PCal-induced end mirror motion during O3.

5. Conclusion

The photon calibrators developed since several years in Virgo and used in a preliminary version during O2, have been improved and used for the first time as a calibration reference during the observation run O3. This allowed to put the relative calibration of the gravitational wave detectors network on the same *absolute* calibration reference: the Gold Standard. The first work of intercalibration between Virgo and LIGO PCal allowed to correct for a discrepancy of 3.92% on the measured laser power between the detectors. A Working Standard for Virgo, similar to the Working Standards used in LIGO and KAGRA, has also been mounted to check the stability in time of the Virgo Integrating Sphere calibration.

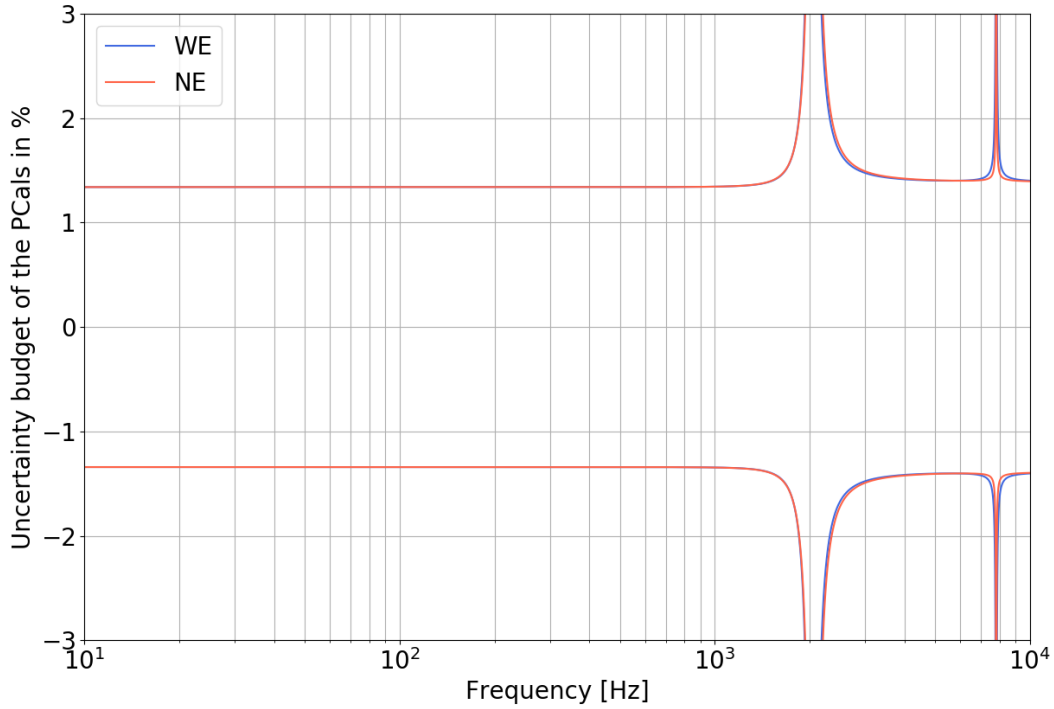


Figure 17: Frequency dependent total uncertainty on the NE and WE end mirrors displacement induced by the photon calibrators for O3a.

On the Advanced Virgo PCal, the laser power has been digitally controlled in order to keep its broadband noise contribution more than 10 times below the sensitivity of the Advanced Virgo interferometer. In addition, the systematic uncertainty on the PCal-induced end mirror motion of the interferometer has been estimated to be 1.35% for both PCal during O3a and 1.39% (resp. 1.73%) on NE PCal (resp. WE PCal) during O3b. There is a common main contribution to the final systematic uncertainty on both PCals: the estimation of the PCal laser power reflected by the end mirror at the level of 1.24%. It will have to be reduced in the future and a first step will be to characterize the calibration of the Virgo Integrating Sphere as a function of the laser beam size. Then, it will be also convenient to use a larger beam on the *injection bench* with a waist located on the interferometer's end mirror so that the beam on the *injection* and *reflection* benches has approximately the same size. Moreover, the Si photodiodes used to estimate the laser power reflected by the end mirror should be replaced by InGaAs photodiodes whose responsivities would have a smaller dependency on temperature variations on the PCal benches. During O3a, the stability of the photodiodes calibration has been estimated to 0.5% on WE and NE PCals but bigger variations, correlated to humidity variations, have been seen on one of the NE photodiode on the *injection* bench. During O3b, NE PD2 calibration stability was updated to 0.6% with variations due to change

in the relative humidity similar to the ones seen during O3a. However WE PD1 calibration started to experience changes during O3b up to 1.1%. This result urged us to increase the systematic uncertainty on the stability of the WE PCal calibration up to 1.2%. The cause of the calibration variations correlated to relative humidity changes has not yet been well understood but investigations are on-going. This phenomenon will have to be addressed in the future to improve the stability in time of the photodiodes calibration.

Not only the amplitude of the PCal-induced displacement needs to be calibrated but also its timing which is a critical feature for coincident data analysis between the different gravitational wave detectors. Using the LED flashing a 1PPS signal on the PCals photodiodes the *absolute* timing of the PCal-induced motion has been measured to $110 \pm 3 \mu\text{s}$ and taken into account in the reconstruction of the gravitational wave signal.

The future improvements foreseen for the PCal stability or for the PCal laser reflected power accuracy will help reducing the uncertainty of the online $h(t)$ provided to data analysis. For the next observing runs, we can expect to reach and keep below 1% the uncertainty for the PCal-induced displacement of the end mirrors.

Acknowledgements

The authors gratefully acknowledge the University of Grenoble Alps Excellence Initiative (IDEX) and the United States National Science Foundation (NSF) for funding the D. Estevez travel grant to LIGO Hanford Observatory (LHO). The authors gratefully acknowledge R. L. Savage and Y. Lecoecue for their contribution to the lab measurements performed at LHO for the intercalibration of the LIGO and Virgo PCals. The authors also gratefully acknowledge the Italian Istituto Nazionale di Fisica Nucleare (INFN), the French Centre National de la Recherche Scientifique (CNRS) and the Foundation for Fundamental Research on Matter supported by the Netherlands Organisation for Scientific Research, for the construction and operation of the Virgo detector and the creation and support of the EGO consortium.

References

- [1] Acernese F *et al.* (Virgo collaboration) 2015 *Class. Quant. Grav.* **32** 024001 URL <https://doi.org/10.1088%2F0264-9381%2F32%2F2%2F024001>
- [2] Acernese F *et al.* (Virgo collaboration) 2018 *Class. Quant. Grav.* **35** 205004 URL <https://doi.org/10.1088%2F1361-6382%2Faadf1a>
- [3] Abbott B P *et al.* (LIGO Scientific Collaboration and Virgo Collaboration) 2017 *Phys. Rev. Lett.* **119**(14) 141101 URL <https://link.aps.org/doi/10.1103/PhysRevLett.119.141101>
- [4] Abbott B P *et al.* (LIGO Scientific Collaboration and Virgo Collaboration) 2017 *Phys. Rev. Lett.* **119**(16) 161101 URL <https://link.aps.org/doi/10.1103/PhysRevLett.119.161101>
- [5] Abbott B P *et al.* 2017 *The Astrophysical Journal* **848** L12 URL <https://doi.org/10.3847%2F2041-8213%2Faa91c9>

- [6] Germain V 2017 *De l'etalonnage d'Advanced Virgo a la recherche d'ondes gravitationnelles emises par des coalescences binaires compactes* Ph.D. thesis Universite Grenoble-Alpes
- [7] Estevez D 2020 *Upgrade of Advanced Virgo photon calibrators and first intercalibration of Virgo and LIGO detectors for the observing run O3* Ph.D. thesis Universite Savoie Mont-Blanc
- [8] Bhattacharjee D *et al.* 2020 (*Preprint 2006.00130*) URL <https://arxiv.org/abs/2006.00130>
- [9] Karki S *et al.* 2016 *Review of Scientific Instruments* **87** 114503 ISSN 1089-7623 URL <http://dx.doi.org/10.1063/1.4967303>
- [10] Hild S *et al.* 2007 *Classical and Quantum Gravity* **24** 56815688 ISSN 1361-6382 URL <http://dx.doi.org/10.1088/0264-9381/24/22/025>
- [11] LIGO Pcal Group 2018 URL <https://dcc.ligo.org/LIGO-T1900097>
- [12] Cahillane C *et al.* 2017 *Phys. Rev. D* **96**(10) 102001 URL <https://link.aps.org/doi/10.1103/PhysRevD.96.102001>
- [13] Taylor B N and Kuyatt C E 1994 *NIST technical document 1297* URL <https://emtoolbox.nist.gov/Publications/NISTTechnicalNote1297s.pdf>